Article

A Targeted Chemo-Photodynamic Combination Platform Based on the DOX Prodrug Nanoparticles for Enhanced Cancer Therapy

Yumin Zhang, Fan Huang, Chunhua Ren, Lijun Yang, Jianfeng Liu, Zhen Cheng, Liping Chu, and Jinjian Liu

ACS Appl. Mater. Interfaces, **Just Accepted Manuscript** • DOI: 10.1021/acsami.7b00927 • Publication Date (Web): 05 Apr 2017

A Targeted Chemo-Photodynamic Combination Platform Based on the DOX Prodrug Nanoparticles for Enhanced Cancer Therapy

Yumin Zhang[1#], Fan Huang[1#], Chunhua Ren[1], Lijun Yang[1], Jianfeng Liu[1], Zhen Cheng[2], Liping Chu[1], Jinjian Liu[1 *]*

[1] Tianjin Key Laboratory of Radiation Medicine and Molecular Nuclear Medicine, Institute of Radiation Medicine, Chinese Academy of Medical Science & Peking Union Medical College, Tianjin 300192, P.R. China.

[2] Molecular Imaging Program at Stanford (MIPS), Department of Radiology and Bio-X Program, Canary Center at Stanford for Cancer Early Detection, Stanford University, Stanford, California 94305, United States.

ABSTRACT: Chemo-photodynamic combination therapy has been received widespread attention in cancer treatment due to its excellent characteristics, such as reducing the adverse side effects of chemo-drugs and improving the therapeutic effects for various cancers. In this study, RGD and DOX was conjugated to PEG by thiol-ene addition and schiff's base reaction, respectively, to prepare the targeted and pH-sensitive anti-tumor prodrug nanoparticles (RGD-PEG-DOX NPs, RGD-NPs). Subsequently, the photosensitizer chlorin e6 (Ce6) was encapsulated into RGD-NPs, thus obtaining a simple and efficient chemo-photodynamic combination platform (RGD-PEG-DOX/Ce6 NPs, RGD-NPs/Ce6). This nanoparticle possessed high drug loading property of both the chemo-drug and photosensitizer and could simultaneously release them under the mild acidic microenvironment of cancer cells, which was expected to realize the synchronization therapy of chemotherapy and photodynamic therapy (PDT). Compared with free DOX and Ce6, RGD-NPs/Ce6 could significantly improve the cellular uptake capacities of DOX and Ce6, resulting in the increased contents of ROS in cancer cells and effective cytotoxicity for tumor cells (MDA-MB-231 cells and MCF-7 cells) upon a laser radiation. The *in vivo* experiment showed that RGD-NPs/Ce6 displayed superior tumor targeting, accumulation and retention ability than the other groups (free DOX, free Ce6 and NPs/Ce6), and thus significantly enhancing the anti-tumor effect *in vivo* with a laser radiation. In addition, the cardiotoxicity induced by DOX was thoroughly wiped out after being loaded and delivered by the nanoparticles according to the pathological analysis. Therefore, the targeted chemo-photodynamic combination therapeutic platform maybe a promising candidate for enhanced cancer therapy.

KEYWORDS: *DOX prodrug nanoparticles, cancer targeting, pH-responsive, codelivery, chemo-photodynamic Combination therapy*

■ INTRODUCTION

With the significant increase of cancer incidence and mortality in China since 2010,[1] cancers have been the leading cause of death. Although the burgeoning anti-tumor techniques such as immunotherapy and photothermal therapy[2-5] have been developed to treat cancer, traditional chemotherapy is still the main therapeutic method for cancer therapy under the current situation.[6-9] Doxorubicin (DOX) with anthracycline antibiotics, as a kind of most highly effective anti-tumor chemotherapeutic drug, is a widely used in clinic which can inhibit the synthesis of DNA and RNA. However, the rapid blood clearance rate and irreversible cardiotoxicity has seriously limited its further development and appilication in clinic.[10-12] In order to overcome these barriers, nanocarriers for drug delivery system (NDDS) such as hydrogels,[13-14] micelles,[15-16] nanofibers[17-18] and nanoparticles[19-21] have been developed and applied. They can improve the pharmacokinetics behaviors of DOX and bring tumor targeting capability.[22-25] For example, the half-life of DOX loaded by PEG_{5K}-Fmoc-VE_2 micelles was increased to forth times at least, and then improved the anti-tumor efficiency. [25] Furthermore, according to the unique characteristics of novel NDDS, they can also act as the chemotherapeutic combination platform by simultaneously loading and delivering two or more drugs, this strategy can boost the chemotherapeutic efficiency and reduce drug resistance at the same time.[26-28] In addition, the novel NDDS could also provide a therapeutic combination platform for various therapy strategies, such as chemo-radiotherapy and chemo-photodynamiccombination therapy.[29,30]

In the recent years, photodynamic therapy (PDT) has been widely applied to treat various tumors as a result of its smaller surgical trauma, better selectivity from normal tissues and capability of repeatable treatment[30-32]. In the process of PDT, the photosensitizer play an important role in producing highly reactive singlet oxygen ($^1O_2$) upon photoexcitation. $^1O_2$ can interact with adjacent biological macromolecules by oxidative reaction and thus lead to cell apoptosis in the targeted sites.[33-34] However, there are some barriers for PDT in the revolution of anti-tumors field, including the low solubility and poor tumor targeted accumulation of the photosensitizer. Therefore, it is very necessary to improve the bioavailability of photosensitizer to achieve desirable anti-tumor effects for PDT. To this end, various NDDS have been reported to deliver the photosensitizer and enhance the PDT efficiency.[35-36] For example, professor Zhu reported a combination of chemotherapy and PDT utilizing a drug delivery system based on inorganic nanoparticles to improve cancer treatment and reduce cisplatin resistance.[35] Nevertheless, the accumulation into tumor tissues of these nanoparticles remained to be solved during the PDT treatment. One method is to formulate targeted nanoparticles by introducing a targeting ligand. Some targeting ligands can specifically bind to receptors on the cancer cells surface and mediate cancer cells' endocytosis of nanoparticles. It was well known that the surface of cell membrane for different kinds of tumors exist some over-expressed receptors.[37-38] Neuropilin-1 receptor is a kind of them, which is a transmembrane protein and play a dominant role in angiogenesis and vascular permeability.[39] Cys–Arg–Gly–Asp–Lys (CRGDK) is a tumor-penetrating peptide that can specially bind to neuropilin-1 receptor, which can improve the accumulation and retention effect of NDDS after covalent modification. Liang's group proved

that cytotoxicity and uptake efficiency of the CRGDK targeted nanocarrier was superior to that of non-targeted nanocarrier. [40-41]

Herein, encouraged by the recent progress and in order to solve the barriers of chemotherapeutic drug and photosensitizer, we developed a targeted chemo-photodynamic combination platform (RGD-NPs/Ce6) based on our previous works.[42] It was obtained by the self-assembly of the targeted DOX prodrug nanoparticle (RGD-PEG-DOX) and photosensitizer chlorin e6 (Ce6). DOX was acted as the hydrophobic part of the platform and Ce6 was efficiently encapsulated in it. The platform has high drug loading ability due to the fact that DOX directly acted as the hydrophobic part. It can hide the anti-tumor activity of DOX and photo-sensitiveness of Ce6 before being activated, because they will not leak under the normal physiological conditions because of the π-π interactions. Due to the EPR effect and RGD ligand, RGD-NPs/Ce6 can targeted deliver and gradually accumulate into tumors, then the acid tumor-environment can induce the breakage of the schiff's base bond of RGD-PEG-DOX, resulting in the disassembly and rapid release of DOX and Ce6. Under the condition of targeting laser radiation, the chemotherapy drugs and photosensitizers can develop the combined anti-tumor activities according to their respective anti-tumor mechanisms (Scheme 1). This study will provide a chemo-photodynamic combination platform for cancer therapy with high drug loading, low side effect and enhanced anti-tumor capability.

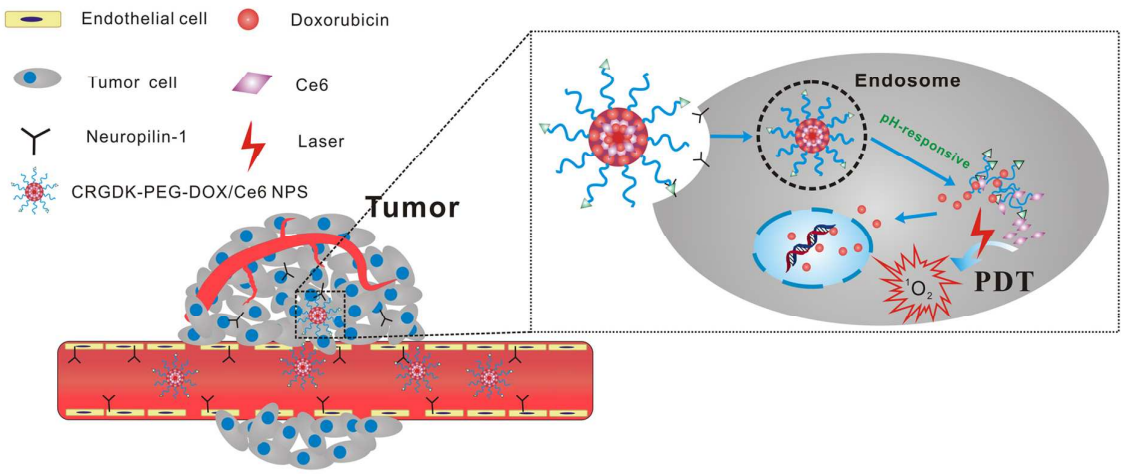

Scheme 1. Design a targeted chemo-photodynamic combination therapeutic platform (CRGDK-PEG-DOX/Ce6 NPs (RGD-NPs/Ce6)) for anti-tumor studies via co-delivering and releasing DOX and Ce6. RGD-NPs/Ce6 was internalized by NRP-1 mediated endocytosis and penetrated into the inner areas of the tumor to kill cancer cells through chemo-photodynamic combination therapy.

■ MATERIALS AND METHODS

Materials. Maleimide-poly(ethylene glycol)-aldehyde (Mal-PEG-CHO) with a PEG molecular weight of 2000 was purchased from Xi'an Ruixi Biological Technology Co., Ltd. (Xi'an, China). Cys-Arg-Gly-Asp-Lys (CRGDK) peptide was obtained from HanBo Biotech (Shanghai, China). Doxorubicin hydrochloride (DOX·HCl) was provided by Wuhan Hezhong Biochem Co., Ltd. (Wuhan, China). 4,6-diamidino-2-phenylindole (DAPI) and Chlorin e6 (Ce6) were purchased from Sigma-Aldrich (St. Louis MO, USA). Other chemical reagents were analytic grade and used without further purification.

Cells and animals. Human breast cancer cell lines MCF-7 (low-Nrp-1 receptor expressing cells) and MDA-MB-231 (Nrp-1 receptor over-expressing cells) were obtained from FDCC (Shanghai, China), which were cultured in Dulbecco's Modified Eagle's Medium (DMEM) with 1% antibiotic solution and 10% fetal bovine serum (FBS). Cell was maintained in a humidified atmosphere containing 5% CO_2 at 37 ℃. The BALB/c nude mice (male, 6-8 weeks) bearing MDA-MB-231 breast tumor model were received from Vital River Laboratory Animal Technology Co., Ltd. (Beijing, China). Mice were acclimated at 55% of humidity and 25 ℃ under natural light/dark conditions before experiment. All the animal experiments were performed in accordance with the protocol approved by Chinese Academy of Medical Science and Peking Union Medical College, and adhered to the Guiding Principles in the Care and Use of Animals of the American Physiological Society.

Synthesis and characterization of the CRGDK-PEG-DOX conjugate. The MAL-PEG-DOX was conjugated by schiff's base between MAL-PEG-CHO and DOX according to our previous work.[29] Briefly, MAL-PEG-CHO (500 mg) and DOX (125 mg) was co-dissolved in 4.0 mL of dimethyl sulfoxide (DMSO), the mixed solution was reacted for 24 h at 40 ℃ under 50 μL of triethylamine catalyzed. Whereafter, CRGDK peptide (200 mg) was directly dissolved into 2.0 mL of DMSO solutions (MAL-PEG-DOX) for 24 h at room temperature. The two kinds of reacted solutions were dialyzed against DMSO to filter the excess and unreacted DOX or CRGDK peptide (MWCO: 1000 Da) under gentle stirring for 48 h, and then dialyzed against PBS to eliminate the DMSO (MWCO: 1000 Da) under gentle stirring for 48 h. The MAL-PEG-DOX and CRGDK-PEG-DOX were obtained after lyophilization, and their structures were characterized by using ^{1}H NMR (Varian INOVA) and UV-vis (Purkinje General). The

molecular weights of MAL-PEG-DOX and CRGDK-PEG-DOX conjugates were determined by using Maldi-TOF MASS (AutoflexIII LRF200-CID, Bruker Daltonics).

Preparation and characterization of PEG-DOX/Ce6 NPs and CRGDK-PEG-DOX/Ce6 NPs. The PEG-DOX/Ce6 NPs (NPs/Ce6) and CRGDK-PEG-DOX/Ce6 NPs (RGD-NPs/Ce6) were prepared via nanoprecipitation method,[43-44] the hydrophobic photosensitizer (Ce6) was loaded into the cores of PEG-DOX NPs and CRGDK-PEG-DOX NPs by hydrophobic interactions. Briefly, Ce6 (2 mg) and PEG-DOX (20 mg) were co-dissolved in DMSO (5 mL) at room temperature, and the organic mixtures were dropwise dispersed into PBS (10 mL) for 24 h under gentle stirring. Then the solution was dialyzed against PBS with a dialysis bag (MWCO: 1000 Da) to remove the DMSO for 72 h, and then filtered through a 450 μm pore-sized membrane. The RGD-NPs/Ce6 was performed in the same method. The hydrodynamic size and morphology of resulting nanoparticles at a concentration of 2.0 mg/mL were characterized by TEM (JEM-2100F) and DLS (Malvern Zetasizer Nano ZS), respectively. The drug loading content of DOX and Ce6 in NPs/Ce6 and RGD-NPs/Ce6 were determined by VARIOSKAN FLASH microplate reader (THERMO SCIENTIFIC) at 488 nm and 670 nm , respectively.

Critical Micelle Concentration (CMC) measurement. The CMC of NPs/Ce6 and RGD-NPs/Ce6 were measured using the pyrene as the fluorescence probe. Concisely, 100 μL of 4 μg/mL pyrene acetone solution was added into NPs/Ce6 and RGD-NPs/Ce6 with different concentrations for 12 h incubation under gentle stirring. The fluorescence spectra of the emission wavelengths of 384 nm and 373 nm of all samples were measured via a fluorescence spectrophotometer at 336 nm excitation wavelength. The CMC of NPs/Ce6 and RGD-NPs/Ce6

were the crossover point in the plots of the fluorescence intensity ratio of 384 nm and 373 nm to the logarithm concentration.

***In vitro* DOX and Ce6 release.** The release kinetic behaviors of DOX and Ce6 from NPs/Ce6 and RGD-NPs/Ce6 were measured using the dialysis bag methods. In detail, 5 mL of NPs/Ce6 and RGD-NPs/Ce6 (1.0 mg/mL) were placed into dialysis bags (MWCO: 3500 Da) and incubated in 30 mL of different pH values solutions (pH 5.0, 6.5, 7.4) at 37 °C under gentle stirring. Quantitative buffer solutions (5 mL) was withdrawn and added by fresh buffer solutions at predetermined time intervals, the accumulative concentration of released DOX and Ce6 from NPs/Ce6 and RGD-NPs/Ce6 were measured by HPLC-UV at 480 nm and fluorescence spectrophotometer at 670 nm, respectively. The released kinetic curves of DOX and Ce6 from NPs/Ce6 and RGD-NPs/Ce6 were drawn according to the accumulative amount of different time point, each sample was conducted in triplicate. Meanwhile, 2.0 mL of RGD-NPs/Ce6 (1.0 mg/mL) was placed into acidic environment (pH 5.0) for incubated 24 h, the structure change of the sample was investigated by TEM.

***In vitro* cellular uptake.** The cellular uptake behavior of NPs/Ce6 and RGD-NPs/Ce6 in MDA-MB-231 and MCF-7 cells were investigated by using the fluorescence microscopy. The MDA-MB-231 and MCF-7 cells were seeded into 12-well plate with a density of 10^5 cells/well, and incubated with DMEM and 10% FBS mixtures in a humidified atmosphere containing 5% CO_2 at 37 °C for 24 h. Then the culture medium was replaced by DMEM with different concentration of NPs/Ce6 and RGD-NPs/Ce6, free DOX and Ce6 were used as the controls. After 4 h incubation, the mixture in each well was dumped, and washed three times with PBS. The cell nucleus were stained by 4,6-diamidino-2-phenylindole (DAPI) on the basis of the

protocol in the staining kit. The Ce6 and DOX signal were recorded by fluorescence microscopy at excitation of 540 nm and 633 nm, respectively. The DAPI was reported at excitation of 405 nm.

For flow cytometric analyses, the MDA-MB-231 and MCF-7 cells were seeded into 24-well plate with a density of 10^5 cells/well, and incubated with DMEM and 10% FBS mixtures in a humidified atmosphere containing 5% CO_2 at 37 °C for 24 h. NPs/Ce6, RGD-NPs/Ce6, free DOX and free Ce6 were incubated with MDA-MB-231 and MCF-7 cells for 1, 4, 8 h, respectively. PBS was used as the blank control. After washing three times with cold PBS, cells were collected for quantitative detected by flow cytometer on a FACS Calibur (BD Accuri C6).

Cellular ROS detection during irradiation. The ROS production in MDA-MB-231 cells by staining methods with DCFH-DA during laser irradiation. The MDA-MB-231 cells were seeded into 6-well plate with a density of 5×10^4 cells/well and cultured in a humidified atmosphere containing 5% CO_2 at 37 ℃ for 24 h. Cells were further incubated with free Ce6, NPs/Ce6 and RGD-NPs/Ce6 (at Ce6 equivalent dose of 20 μg/mL) for 24 h. After incubated with 20 μM DCFH-DA for 20 min, 6-well plates were irradiated using a laser with a power of 50 mW /cm^2 for 5 min. The fluorescence signals of DCF inside cells were recorded by fluorescence microscopy at excitation of 488 nm and at emission of 525 nm.

The ROS contents of various Ce6 formulations in cancer cells were also quantitatively determined. The MDA-MB-231 and MCF-7 cells were seeded into 96-well plate with a density of 5×10^3 cells/well and cultured in a humidified atmosphere containing 5% CO_2 at 37 ℃ for 24 h. Then the culture medium was replaced by DMEM with PBS, free Ce6, NPs/Ce6 and

RGD-NPs/Ce6 (at Ce6 equivalent dose of 20 μg/mL) for further incubation of 24 h. 20 μM DCFH-DA were added into wells for incubating 20 min and irradiated utilizing a 633 nm He-Ne laser at a power of 50 mW/cm^2 for 5 min or not. Subsequently, the fluorescence intensity of DCF in each well was quantitative detected by a fluorescence microplate reader (Thermo Scientific, Varioskan Flash).

In vitro **Cell cytotoxicitys.** The cell cytotoxicity of NPs/Ce6 and RGD-NPs/Ce6 were determined by MTT assay with MDA-MB-231 and MCF-7 cells in dark condition. Briefly, MDA-MB-231 and MCF-7 cells were cultured for 24 h, then culture medium were discarded, and a series of DOX concentration of free DOX, NPs/Ce6 and RGD-NPs/Ce6 were added into corresponding wells and incubated for 24 h. The drug solution in each well was replaced by 20 μL of MTT solution. After 4 h incubation, the absorbency of the medium solution was measured on a microplate reader at 570 nm. The cell viability was expressed by (sample/control) × 100%. All data were presented as mean ± SD (n = 6).

The chemo-photodynamic combination antitumor efficiency of NPs/Ce6 and RGD-NPs/Ce6 were also measured by MTT assay with MDA-MB-231 and MCF-7 cells. After incubation for 24 h, culture medium were discarded, and a series of Ce6 concentration of free Ce6, NPs/Ce6 and RGD-NPs/Ce6 were added into corresponding wells and incubated for 12 h in dark condition, the 96-well plate was placed into superstratum of incubator, the laser source was adjusted and fixed into the underneath of 96-well plate. We should adjust the distance of laser source to keep the whole 96-well plate being irradiated with the same irradiated power. Afterwards, the 96-well plates were irradiated by a 633 nm laser device at a power of 50 mW cm^{-2} for 5 min. After additional 12 h of incubation, the mediums were replaced by 20 μL of MTT solution. After 4 h

incubation, the absorbency of the medium solution was measured on a microplate reader at 570 nm. The cell viability was expressed by (sample/control) × 100%. All data were presented as mean ± SD (n = 6).

Tumor-targeting accumulations, retention in tumor bearing mice. The mice bearing MDA-MB-231 breast tumor were divided into free Ce6, NPs/Ce6 and RGD-NPs/Ce6 three groups when tumor volume reached about 200 mm^3. Mice were injected intravenously via tail vein at equivalent Ce6 dose of 2.0 mg/kg body weight. At designed time points (1, 6, 12, 24 h), the mice were anesthesiaed by isoflurane, the fluorescence images *in vivo* were obtained by Kodak IS *in vivo* imaging system through the fluorescence of Ce6 with an excitation wavelength of 633 nm and an emission wavelength of 790 nm. At 24 h post injection, the mice were sacrificed, the tumor and main organs (heart, liver, spleen, lung, and kidney) were dissected for *ex vivo* imaging. In order to investigate the tumor penetrating ability of NPs/Ce6 and RGD-NPs/Ce6, we collected the tumor tissues and fixed it with 4% paraformaldehyde at 4 °C for 24 h, and then embedded in paraffin, cut 3 μm thick sections and mounted onto microscopic slides, the sections were stained with DAPI at 20 μg/mL for 20 min. Ce6 in tumor tissues was observed by fluorescence microscope (Leica, DMI6000B).

Anti-tumor efficacy of RGD-NPs/Ce6 in tumor bearing mice. The *in vivo* chemo-photodynamic combination treatment of RGD-NPs/Ce6 and NPs/Ce6 were performed by MDA-MB-231 tumor bearing mice. When the tumor volume reached 100 mm^3, the tumor bearing mice were divided into seven groups, each group had eight animals, and treated with PBS, free Ce6 (2 mg/kg) upon laser irradiation, free DOX (5 mg/kg), RGD-NPs/Ce6 and NPs/Ce6 (equivalent DOX of 5 mg/kg, equivalent Ce6 of 2 mg/kg) with or without laser

irradiation via tail vein for five times in two weeks, respectively. After 12 h of each injections, for the irradiated groups, mice were irradiated using a laser (200 mW/cm^2, 10 min), respectively. The body weight and tumor volumes were measured every two days during treatment. On days 20, the mice were sacrificed, tumors and main organs (heart, liver, spleen, lung, kidney) were dissected and further studied after H&E staining to monitor the morphological and pathological feathers of organs.

Statistical analysis. SPSS 19.0 software were used for the statistical analyses. All data were rendered as mean ± standard deviation values. The statistical significance of differences was determined by Student's *t* test. *P<0.05, **P<0.01 were used for statistical difference and significant difference, respectively.

■ RESULTS AND DISCUSSIONS

Synthesis and characterization. The targeted DOX prodrug conjugate CRGDK-PEG-DOX was synthesized through the combined methods of Schiff's base reaction and thiol-ene amidation. The synthetic route was shown in Fig. S1. Compared the ^{1}H NMR spectrum in Fig. 1A and Fig. 1B, DOX was used as control (Fig. S2), it could find that after reacted with amino group (NH_2) of DOX, the peak of aldehyde group (-CHO) in the MAL-PEG-CHO was disappeared while the typical peak of DOX was generated in the product, which confirmed the successfully synthesized of MAL-PEG-DOX by schiff base reaction. Then, from the Fig. 1C we could find the disappearance of typical peak of MAL after the reaction between MAL-PEG-DOX and CRGDK peptide, indicating the successful conjugation of CRGDK-PEG-DOX. The UV-Vis data (Fig. 1D) further proved the successful synthesis of CRGDK-PEG-DOX as evidenced by the visible absorption peak at 210 nm for CRGDK peptide and 488 nm for DOX.The molecular weight of

MAL-PEG-DOX and CRGDK-PEG-DOX conjugate was 2543.09 and 3120.13, respectively (Fig. S3).

The targeted chemo-photodynamic combination platform RGD-NPs/Ce6 was prepared by nanoprecipitation method, and NPs/Ce6 was taken as control. The size and morphology of these two nanoparticles were measured by the DLS and TEM. As shown in Fig. 2, both of NPs/Ce6 and RGD-NPs/Ce6 self-assembled into spherical structures, and the diameters of them were 131±3.5 nm and 145±5.3 nm with narrow polydispersity index of 0.17±0.03 and 0.199±0.06, respectively. As a control, the PEG-DOX NPs and RGD-PEG-DOX NPs without loading Ce6 also showed spherical structures, and their diameters were 121.7 nm and 134.5 nm, respectively (Fig. S4). This optimized size of prodrug nanoparticles could preferably accumulate and permeate into tumors via EPR effect.[45] Meanwhile, they have a good stability without any aggregation or sedimentation in water for at least 48 h (Fig. 2C). The drug loading capacity (DLC) of DOX and Ce6 for the NPs/Ce6 and RGD-NPs/Ce6 were calculated by a standard curve of DOX and Ce6, which were measured by using varian fluorescence spectrophotometer. As summarized in Table 1, the DLC of DOX and Ce6 for RGD-NPs/Ce6 were determined to be as high as 17.95±1.03% and 9.36±0.42%, respectively, which is similar with the NPs/Ce6 (18.53±1.25% for DOX and 9.65±0.53% for Ce6). In addition, the CMC of NPs/Ce6 and RGD-NPs/Ce6 were measured by using pyrene as the fluorescent probe. As shown in Fig. 2D, they were calculated from the first inflection point in the curve of the absorption intensity ratio of I_{384}/I_{373} versus the logarithm of concentration. The CMC of NPs/Ce6 and RGD-NPs/Ce6 were 4.15 and 4.22 μg/mL approximately. The similar DLC and CMC of these two kinds of nanoparticles were because of their same DOX hydrophobic segments.

Table 1. Characterization of NPs/Ce6 and RGD-NPs/Ce6

Sample	Diameter[a] (nm)	PDI	ζ (mV)	DLC of DOX (%)	DLC of Ce6 (%)
NPs/Ce6	131±3.5	0.17±0.03	-3.4±0.35	18.53±1.25	9.65±0.53
RGD-NPs/Ce	145±5.3	0.19±0.06	-2.2±0.15	17.95±1.03	9.36±0.42

[a] Determined by using a DLS at 25 °C in PBS (10 mM, pH 7.4). PDI = size and size distribution; ζ= zeta potential; DLC = drug-loaded content. Data represented mean±SD (n = 3).

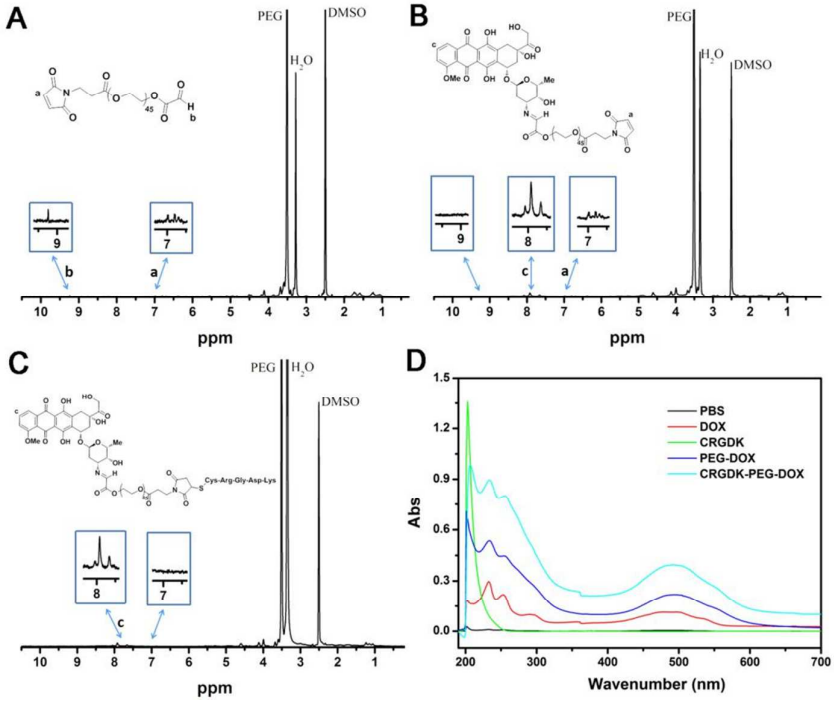

Fig. 1. ^{1}H NMR spectra of MAL-PEG-CHO (A), MAL-PEG-DOX (B) and CRGDK-PEG-DOX (C). DMSO-*d*6 was used as the solvent. (D) Uv-Vis spectrum of DOX, CRGDK, PEG-DOX, and CRGDK-PEG-DOX. PBS was utilized as control.

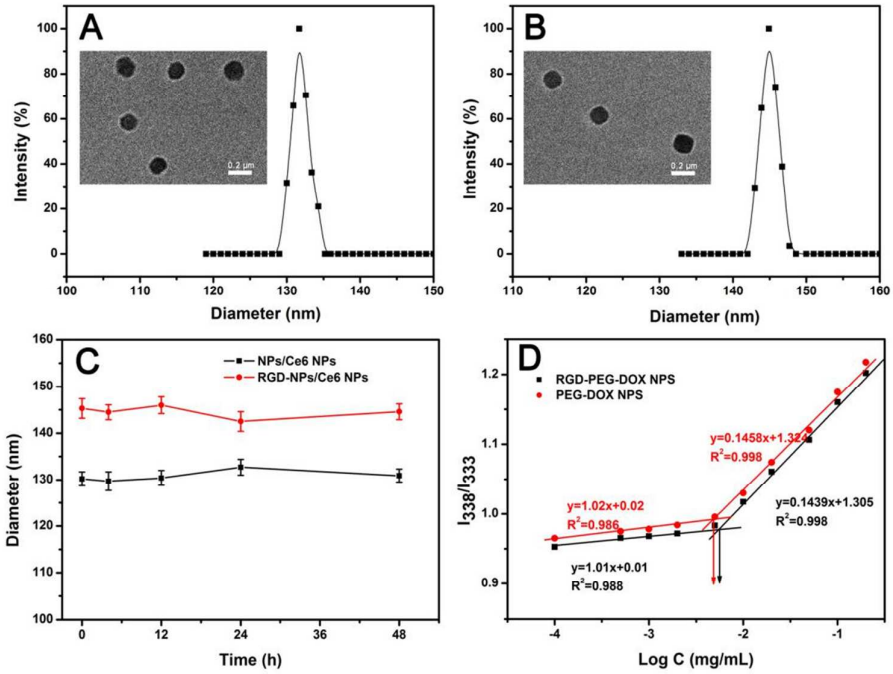

Fig. 2. Characterization of NPs/Ce6 and RGD-NPs/Ce6. The DLS and TEM results of NPs/Ce6 (A) and RGD-NPs/Ce6 (B); the stability of NPs/Ce6 and RGD-NPs/Ce6 in waters (C); the CMC of NPs/Ce6 and RGD-NPs/Ce6 (D).

***In vitro* DOX and Ce6 release.** The drug release behaviors of NPs/Ce6 and RGD-NPs/Ce6 were studied by mimicking the slightly acid pH of the endosomal (~6.5) and lysosomal (~5.0) compartments at 37°C with dialysis method *in vitro*.[44] As shown in Fig. 3A and 3B, less than 10% of drug was released from NPs/Ce6 and RGD-NPs/Ce6 at pH 7.4, which further proved the favorable structural stability and drug loading stability. However, about 30% of DOX and Ce6 were released from NPs/Ce6 and RGD-NPs/Ce6 at pH 6.5 within 4 h, and almost 70% of DOX and 80% of Ce6 released from these two nanoparticles at pH 5.0 within 24 h, confirming the great pH-sensitivity of the nanoparticles which was due to the breakage of schiff's base bond in them under the acid environment. The similar release kinetics between DOX and Ce6 of the two nanoparticles might be ascribed to the fact that DOX was directly

acted as the hydrophobic parts of the prodrug nanoparticles and Ce6 was loaded in it depended the hydrophobic and π-π interactions between them, this resulted the simultaneously liberated once the nanoparticles were disintegrated.

Meanwhile, the NPs/Ce6 and RGD-NPs/Ce6 showed the similar drug release behaviors, which was attributed to the same hydrophobic segments (DOX as the hydrophobic parts of prodrug nanoparticles) and the same release mechanism. In addition, the fluorescence spectral change of Ce6, NPs/Ce6 and RGD-NPs/Ce6 in the acidic PBS (pH 5.0) could also confirmed responsiveness and high acid sensitivity of the prodrug nanoparticles (Fig. 3C). Furthermore, the morphology of the nanoparticles was collapsed and irregularly aggregated together after incubation in acidic PBS (pH 5.0) for 24 h (Fig. 3D) . These results revealed that our designed prodrug nanoparticles could offer a platform to synchronously release DOX and Ce6 at the acid environment of tumor tissues.

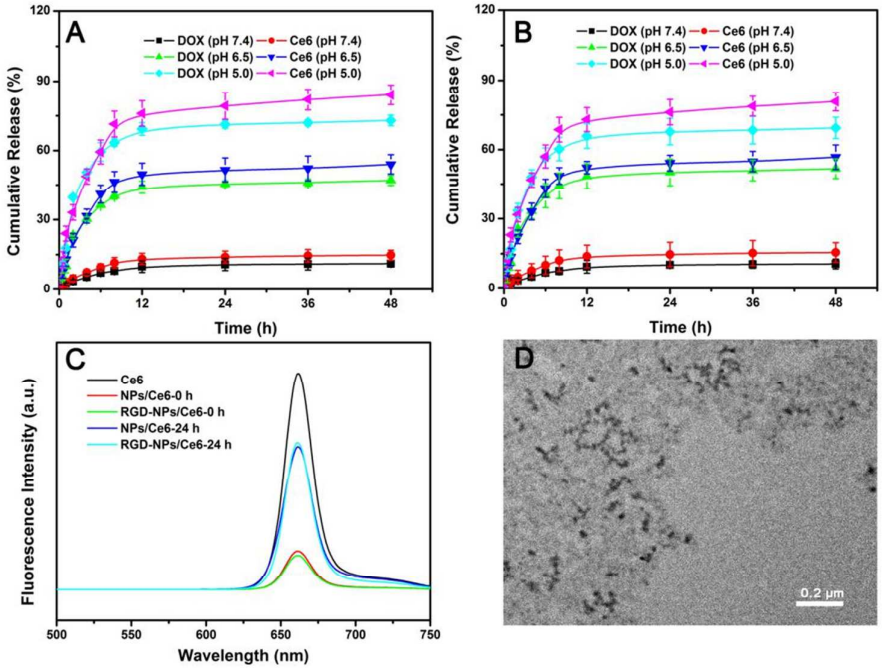

Fig. 3. Drug release characterization of NPs/Ce6 and RGD-NPs/Ce6. The drug release behaviors of NPs/Ce6 (A) and RGD-NPs/Ce6 (B); the fluorescence spectral change of Ce6, NPs/Ce6 and RGD-NPs/Ce6 in the acidic PBS (C); The morphology change of RGD-NPs/Ce6 after incubation for 24 h at pH 5.0 (D).

Cellular uptake. The cellular uptake of NPs/Ce6 and RGD-NPs/Ce6 were investigated in MDA-MB-231 and MCF-7 cells by using fluorescence microscopy based on the green fluorescence of DOX and red fluorescence of Ce6 (for distinguishing the intracellular distribution of two drugs, clearly). As shown in Fig. 4, the green fluorescence of free DOX distributed the whole nucleus of MDA-MB-231 cells after incubation for 4 h (Fig. 4A), but the fluorescence intensity of DOX in the cells significantly decreased as the incubation time elapsed (Fig. 4B), this was because of its easily diffused through the cellular membrane, leading to the quickly clearance and shortly retention time in cells of free DOX.[46-47] Nevertheless, for free Ce6 group, the lower and darker red fluorescence signals was seen in MDA-MB-231 cells, showing that less Ce6 was internalized by cancer cells, which might be ascribed to the passive diffusion through the cell membrane of free Ce6, and further resulted in the poor photodynamic therapeutic efficacy.[48-49] In contrast, the Ce6 fluorescence intensity in MDA-MB-231 cells was obviously increased for NPs/Ce6 and RGD-NPs/Ce6 group, indicating that the cellular uptake capacity of Ce6 was promoted after loaded and delivered by NPs/Ce6 and RGD-NPs/Ce6.

Meanwhile, the NPs/Ce6 and RGD-NPs/Ce6 could keep the fluorescence intensity of DOX and Ce6 sustained growth in MDA-MB-231 cells after incubation for 8 h, which showed significant differences compared with free DOX and free Ce6 (Fig. 4B and 4C). In addition,

comparing the two NPs groups, we found that the fluorescence intensity (both red and green) of RGD-NPs/Ce6 was much stronger than that of NPs/Ce6 in MDA-MB-231 cells, while it couldn't find these significant differences in MCF-7 cells (low-Nrp-1 receptor expressed) (Fig. S5), suggesting that the RGD-NPs/Ce6 could be specifically internalized by NRP-1 mediated uptake in the Nrp-1 receptor over-expressing cells.[50]

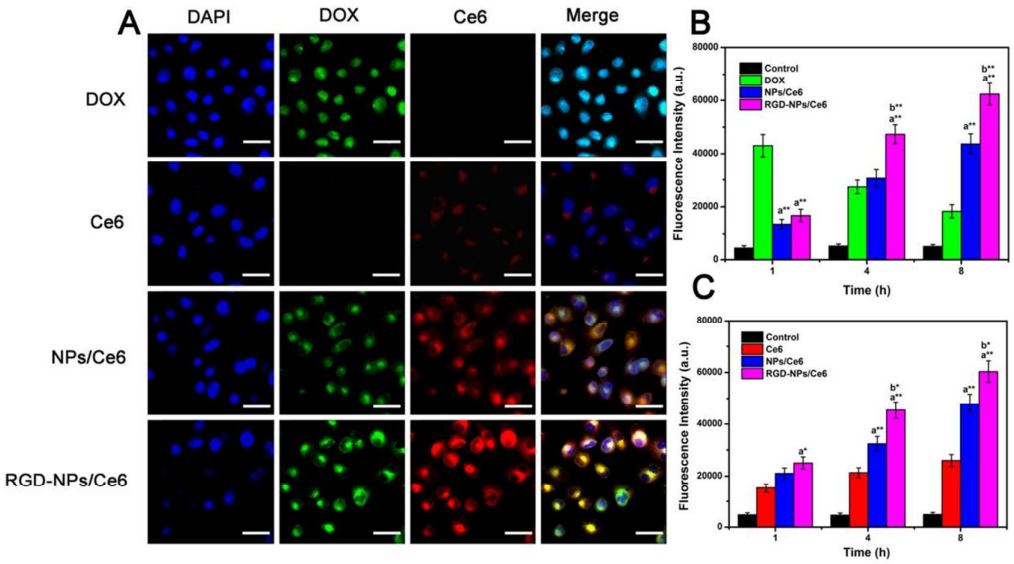

Fig. 4. Cellular uptake of NPs/Ce6 and RGD-NPs/Ce6 in MDA-MB-231 cells. The Cellular uptake of NPs/Ce6 and RGD-NPs/Ce6 in MDA-MB-231 cells observed by fluorescence microscopy after incubation for 4 h (A). Scale bar = 25 μm; quantitative analysis of mean fluorescence intensity of DOX (B) and Ce6 (C) after incubated with free drugs, NPs/Ce6 and RGD-NPs/Ce6 for 1, 4, and 8 h via flow cytometry. (*P<0.05, **P<0.01, a = in comparison with free DOX or Ce6, b = in comparison with NPs/Ce6).

ROS measurement during PDT. The ROS contents of Ce6 produced actually decreased after being loaded by NPs and RGD-NPs (Fig. S6A). This could be explained by the phenomenon in Fig. 3C that the quenched fluorescence signals of Ce6 in RGD-NPs/Ce6

resulted in the reduction of photosensitivity and ROS production. Afterwards, as the cellular uptake capacity of Ce6 was improved after being loaded by NPs/Ce6 and RGD-NPs/Ce6, we investigated whether the ROS contents in cancer cells would be increased under laser radiation. The intracellular ROS production in MDA-MB-231 cells incubated with different Ce6 formulations was recorded and imaged by a green fluorescence (DCFH-DA). As shown in Fig. 5A, the ROS fluorescence intensity produced by free Ce6 with or without laser radiation was very low, which was due to the poor ability of cellular uptake. The ROS produced by Ce6 did not show obvious significance compared with PBS (0 μg/mL) until the concentration of Ce6 was above 50 μg/mL (Fig. S6B).

As shown in Fig. 5A, the weakly ROS fluorescence intensity was recorded from the NPs/Ce6 and RGD-NPs/Ce6 in no laser group, which was produced by DOX in the process of chemotherapy. While the ROS fluorescence intensity of NPs/Ce6 and RGD-NPs/Ce6 with irradiation showed a great improvement, which was significantly higher than Ce6 with or without irradiation group. Furthermore, as shown in Fig. 5A, the ROS generated by RGD-NPs/Ce6 was much more than that of NPs/Ce6 after laser radiation in NRP-1 receptor over-expressed MDA-MB-231 cells, which was because that the RGD peptide could specifically recognize NRP-1 receptor, and then resulted in internalization by MDA-MB-231 cells. This result was consistent with the cellular uptake.

As shown in Fig. 5 B and C, both in MDA-MB-231 cells and MCF-7 cells, the poor ROS contents were produced by free Ce6 with or without laser irradiation. However, the ROS concentration of NPs/Ce6 and RGD-NPs/Ce6 under irradiation were much higher than that without irradiation group. Moreover, there was no difference of ROS concentration between

RGD-NPs/Ce6 and NPs/Ce6 treatment with irradiation in MCF-7 cells (Fig. 5C). This may result from the lower NRP-1 receptor expression in MCF-7 cells surface, and then no targeted delivery of Ce6 was achieved.

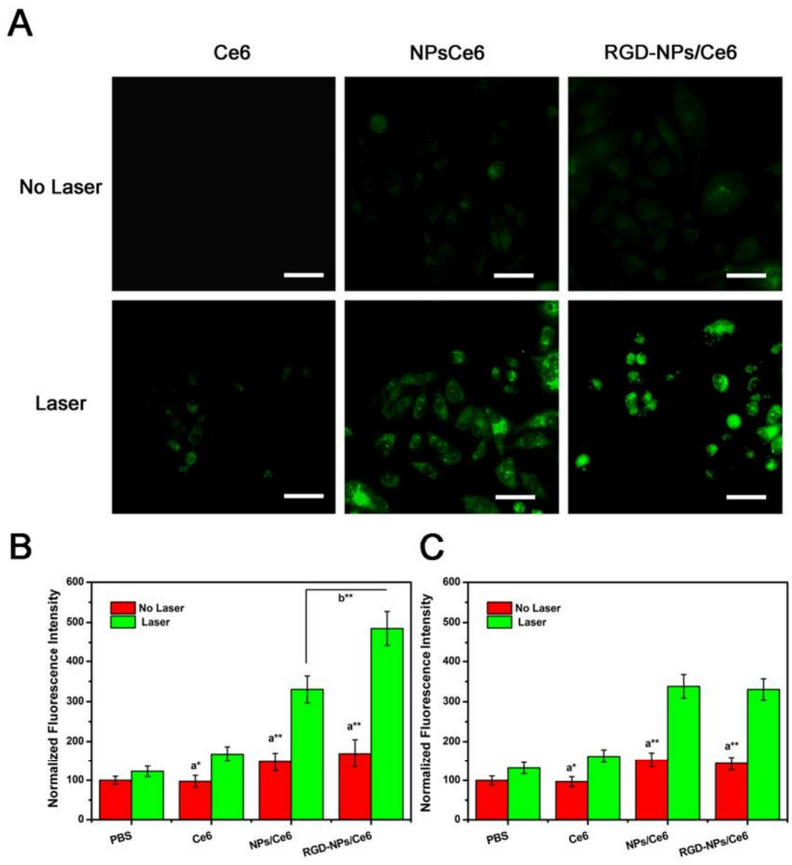

Fig. 5. The intracellular ROS production stained by DCFH-DA after incubated with various Ce6 formulations in MDA-MB-231 cells under a irradiation or not (A). Scale bar = 25 μm; The ROS contents produced by various Ce6 formulations in MDA-MB-231 cells (B) and MCF-7 cells (C). PBS was used as control. (*P<0.05, **P<0.01, a = in comparison with no laser radiation, b = in comparison with NPs/Ce6).

Cytotoxicity assay. We first investigated the *in vitro* anti-tumor effects of chemotherapy using MCF-7 and MDA-MB-231 cells by MTT assay. As shown in Fig. 6A and 6B, the

cytotoxicity of three DOX formulations all showed concentration-dependent profiles. For MCF-7 cells (Fig. 6A), the *in vitro* anti-tumor efficiency of free DOX was higher than NPs/Ce6 and RGD-NPs/Ce6, and when the concentration of DOX was increased to 200 μg/mL, the cytotoxicity of free DOX also showed highest (Fig. S7). This was because of its easily diffused through the cellular membrane, leading to open the anti-tumor function of free DOX.[23-24, 46] Meanwhile, the cell suppression capacity of NPs/Ce6 and RGD-NPs/Ce6 had no obvious difference with the DOX concentration range from 0.1 to 50 μg/mL in the low-Nrp-1 receptor expressing cells. However, the RGD-NPs/Ce6 showed the strongest anti-tumor efficacy in MDA-MB-231 cells (Fig. 6B), even higher than the free DOX group, this could be attributed to the active targeting mediated by RGD, resulting in more and more DOX delivered into MDA-MB-231 cells, and thus achieving higher cytotoxicity.

For the PDT studies *in vitro*, as shown in Fig. 6C and 6D, free Ce6 showed undesirable anti-tumor efficiency in both MCF-7 and MDA-MB-231 cells under laser radiation, resulting from fact that the low concentration of ROS generated by PDT couldn't play an important role in killing cancer cells. This result was consistent with cellular uptake studies and ROS detection. However, the cell viability of NPs/Ce6 and RGD-NPs/Ce6 groups (Fig. 6C and 6D) was much lower than chemotherapy groups (Fig. 5A and 5B) upon laser irradiation for 5min, suggesting that the combination therapy under the irradiation could achieve more striking cancer treatment effect than chemo or photodynamic treatment alone.[31-32] As far as we know, the NPs/Ce6 and RGD-NPs/Ce6 did delivered more Ce6 into the cancer cells, this could ensure the PDT performed, resulting in abundant ROS generation by PDT in cancer cells and accomplishment of the chemo-photodynamic combination therapy with the DOX prodrug

nanoparticles. Furthermore, compared Fig. 6C and Fig. 6D, it could be found that the cytotoxicity of RGD-NPs/Ce6 was much higher in MDA-MB-231 cells than NPs/Ce6. This result and its principle were consistent with chemotherapeutic studies of NPs/Ce6 and RGD-NPs/Ce6.

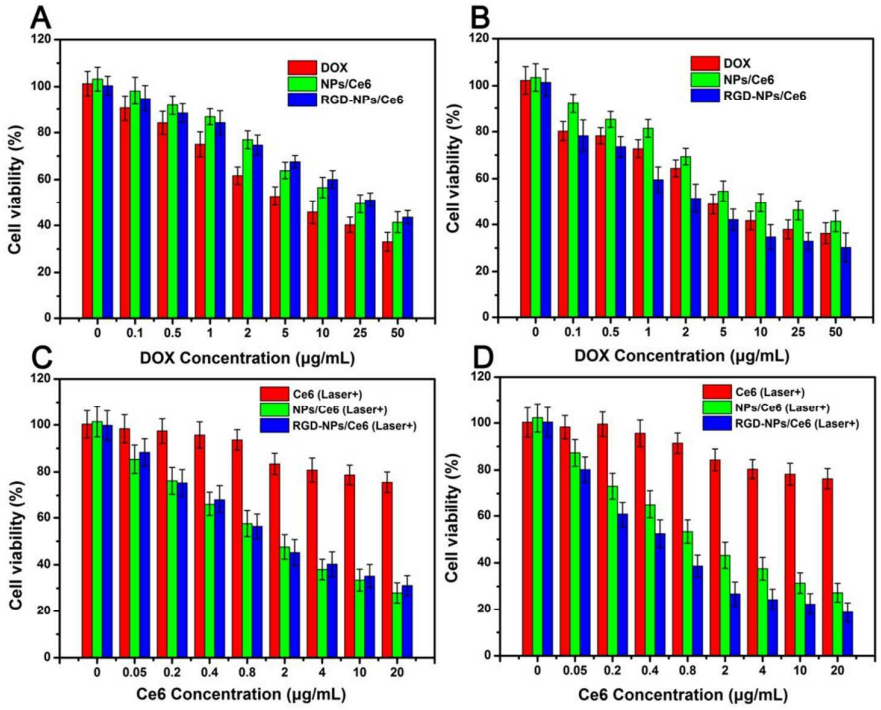

Fig. 6. The cytotoxicitys of different DOX or Ce6 formations against MCF-7 and MDA-MB-231 cells with or without laser radiation. The cytotoxicitys of chemotherapy against MCF-7 cells (A) and MDA-MB-231 cells (B); the cytotoxicitys of chemo-photodynamic combination therapy against MCF-7 cells (C) and MDA-MB-231 cells (D) under laser radiation for 5 min.

Tumor targeting accumulation and retention in tumor bearing mice. The NIR fluorescence of Ce6 could be used as a probe for detecting the tumor accumulation and retention of NPs/Ce6 and RGD-NPs/Ce6 in MDA-MB-231 tumor-bearing nude mice.[32, 34-35,

[50] The *in vivo* distributions of different Ce6 formulations at different time were shown in Fig. 7A, free Ce6 was mainly distributed in liver and bladder after injected 1 h, and most of Ce6 was metabolized within 6 h. The pharmacokinetics studies of free Ce6 (Fig. S8) also proved its rapidly blood clearance kinetics, this resulted in the unsatisfactory tumor accumulation. However, the Ce6 signals of NPs/Ce6 and RGD-NPs/Ce6 showed longer blood circulation and higher accumulation in tumors until administrated 24 h. In detail, the fluorescence signals accumulation of NPs/Ce6 and RGD-NPs/Ce6 were slowly reduced in the liver, and the time dependent clearance curves exhibited prolonged circulation time (Fig. S8). On the other hand, as shown in Fig. 7A, The Ce6 signal of NPs/Ce6 and RGD-NPs/Ce6 in the tumor was gradually increased, and decreased quickly in other organs as time lasted. Thereinto, the fluorescence intensity signal of NPs/Ce6 in the tumors reached a maximum at 12 h post-injection and with a slight decrease after 24 h injection, proposing that the NPs/Ce6 were not subject to rapid metabolism from mice and were excellently accumulated into tumors by the EPR effect.[50, 51] Furthermore, in the initial 1 h, the RGD-NPs/Ce6 treatment showed preferential and higher drug accumulation in tumors compared to the treatment of NPs/Ce6, and could permanently accumulated into tumors until injected 24 h, this was due to the active targeting to Nrp-1 receptors on tumor vascular endothelial cells or tumor cells. After 24 h post-injection, tumors and main tissues of different groups were imaged and quantitative detected by using a Kodak IS *in vivo* imaging system. The results were shown in Fig. 7B and 7C, all of the examined organs showed basal fluorescence signals except of tumors. Obviously, the tumor fluorescence intensity of free Ce6 group was weakest, which was significant difference compared with NPs/Ce6 ($P<0.05$) and RGD-NPs/Ce6 ($P<0.01$),

further proving the poor tumor accumulation of free Ce6.[40, 45] More importantly, it was easily found that the tumor accumulation of RGD-NPs/Ce6 was superior to NPs/Ce6, highlighting the significantly difference between active targeting mediated by Neuropilin-1 receptor and passive targeting mediated by EPR effect. [40, 50, 52]

In addition, the drug retention reconciled by NPs/Ce6 and RGD-NPs/Ce6 were coarsely evaluated by staining the tumor sections with DAPI after 24 h injection. For free Ce6 group, as shown in Fig. 7D, we couldn't find the red fluorescence signals in the tumor sections, because the rapid clearance velocity of Ce6 *in vivo* resulted that it had no sufficient chances to accumulative into tumors, and then the free Ce6 was hard to penetrate into tumor tissues.[51] In contrast, the Ce6 fluorescence in the NPs/Ce6 and RGD-NPs/Ce6 groups were much higher than free Ce6 group, indicating that encapsulating Ce6 by nanoparticles could enhance the drug accumulation and tumorous retention because of the EPR effect. More importantly, the RGD-NPs/Ce6 showed highest Ce6 fluorescence compared with free Ce6 and NPs/Ce6, which was attributed to the Neuropilin-1 recepter mediated targeting of CRGDK peptides.

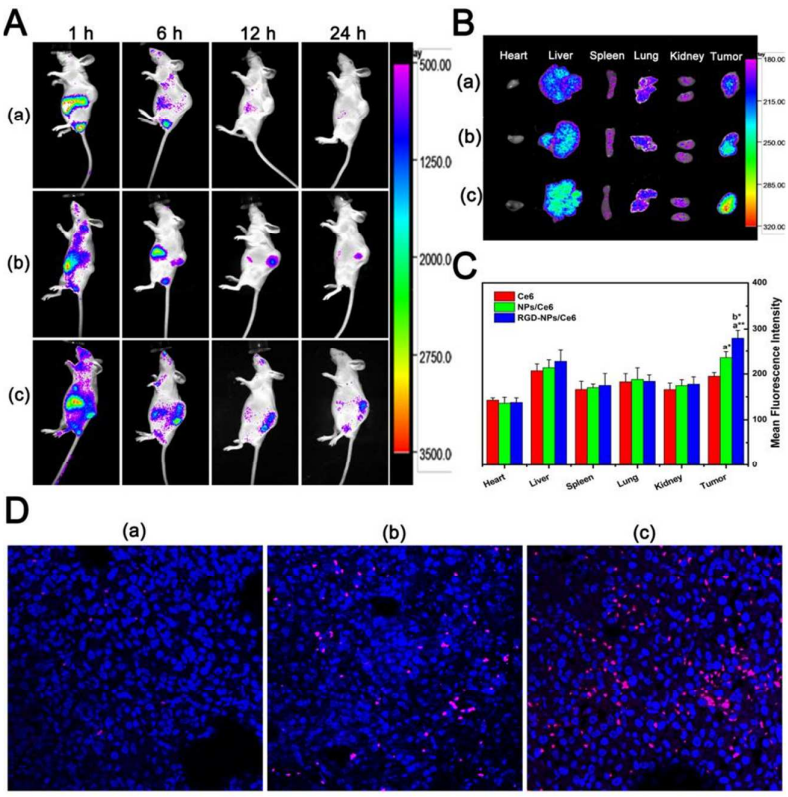

Fig. 7. Drug accumulation and retention studies in MAD-MB-231 tumor bearing nude mice. (A) the real time *in vivo* imaging of various Ce6 formulations in MAD-MB-231 tumor bearing nude mice after intravenous injection (a, b, c represented free Ce6, NPs/Ce6 and RGD-NPs/Ce6, respectively); fluorescent signals of different Ce6 formulations were imaged (B) and quantitative detected (C) in the organs and tumors 24 h post-administration; *In vivo* tumor accumulation and retention of various Ce6 formulations 24 h post-administration (D). (a, b, c represented free Ce6, NPs/Ce6 and RGD-NPs/Ce6, respectively. *P<0.05, **P<0.01, a = in comparison with free Ce6, b = in comparison with NPs/Ce6). Blue: DAPI stained cell nuclei. Red: Ce6 formulations. Original magnification:×40.

Anti-tumor effect studies in MDA-MB-231 tumor-bearing mice. The anti-tumor efficacy of various treatment groups was shown in Fig. 8A, which revealed different degree growth of tumors. In the therapeutic treatment groups, NPs/Ce6 and RGD-NPs/Ce6 groups showed preferable anti-tumor efficiency compared with free DOX group, owing to their prolonged

circulation time and better accumulation in tumors. This was proved in our previous studies.[29, 52] As for free Ce6, because of its fast blood clearance and less tumor accumulation, the tumor growth of free Ce6 treated mice was not suppressed. Upon using laser irradiation, the inhibition effect for tumor growth of Ce6 loaded nanoparticles was better than the others, and RGD-NPs/Ce6 displayed the best inhibition effect. Moreover, the anti-tumor effect was further investigated by using H&E staining (Fig. 8C), in which RGD-NPs/Ce6 with laser irradiation revealed the superior treatment effect with widespread and serious apoptosis and necrosis of the cancer cells under an optical microscope.

The weight changes of various treatment groups during the period of treatments were shown in Fig. 8B, similar variation trends in body weight were observed during the treatment excepted for the DOX group, this group showed a significantly declines owing to a series of toxic and side effect of free DOX. H&E assay was also employed to assess the toxicology of these nanoparticles. As shown in Fig. 9, there was obviously myocardial inflammation in the heart tissues for the DOX group, which was manifested by cytoplasmic relaxation with flake myocardial degeneration, myocardial swelling, myofibril loose and nucleus degeneration.[11-12] However, as shown in Fig. 9 and Fig. S9 (both combination therapy and chemotherapy), mice treated with PBS, Ce6, NPs/Ce6 and RGD-NPs/Ce6, no matter with or without irradiation, showed no obvious signal of damage or toxicity from pathologic analysis of heart, liver, spleen, lung and kidney. Overall, these *in vivo* results demonstrated that the RGD-NPs/Ce6 could act as a targeted chemo-photodynamic combination platform to exhibit enhanced anti-tumor therapeutic efficacy with little side effects.

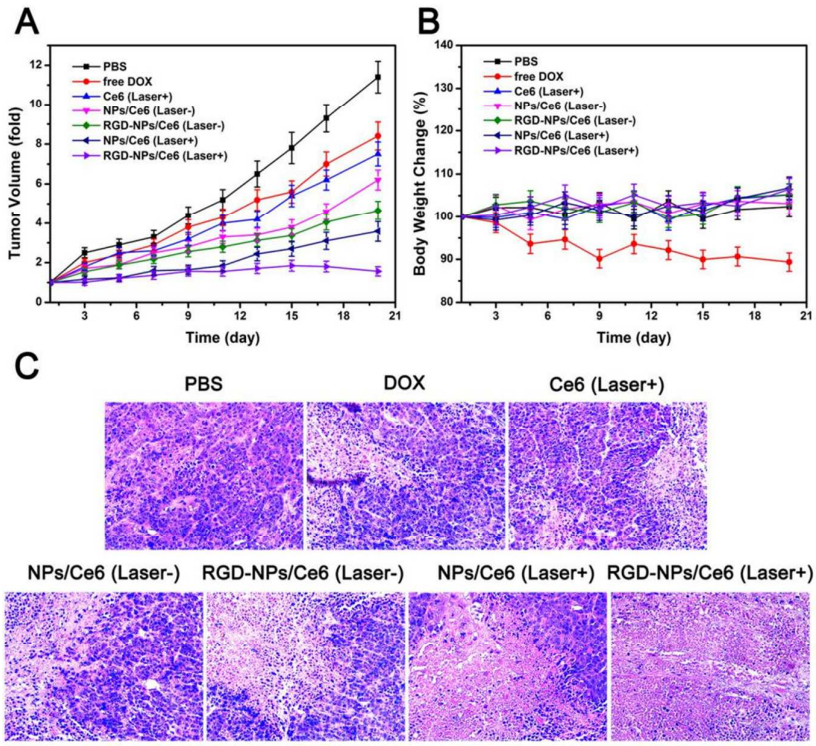

Fig. 8. *In vivo* chemo-photodynamic therapy of RGD-NPs/Ce6 NPs. Tumor volume growth curves (A) and body weight curves (B) of the mice after treatment with free DOX, free Ce6 with laser irradiation or NPs/Ce6 and RGD-NPs/Ce6 with or without laser irradiation. HE stained tumors in the mice treated with various formulations with or without laser radiation (C). Original magnification:×20.

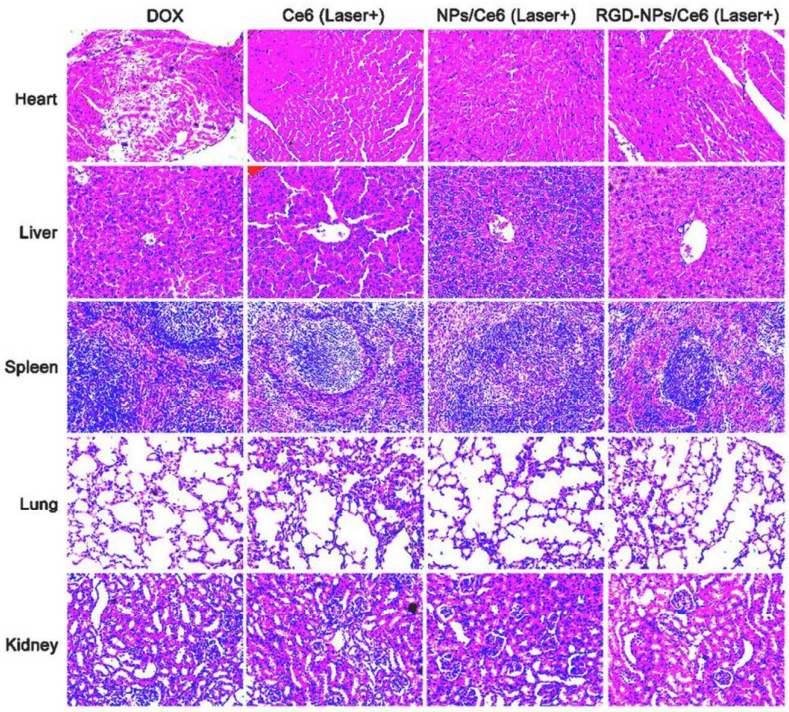

Fig. 9. H&E stained tissue sections from the heart, liver, spleen, lung, and kidney of the nude mice after 20 days post-treatment of chemo-photodynamic combination therapy, DOX and Ce6 with laser radiation as the controls. Original magnification:×20.

■ CONCLUSIONS

In this study, we successfully developed a targeted chemo-photodynamic combination platform based on the DOX prodrug nanoparticles for enhanced anti-tumor effect. In this platform, the photosensitizer Ce6 was entrapped by pH-sensitive DOX prodrug nanoparticles which was decorated CRGDK peptides on their PEG shell. RGD-NPs/Ce6 could simultaneously release DOX and Ce6 under the mild acidic microenvironment of tumors, so that accomplished the chemotherapy and PDT synchronously. Compared with free DOX and Ce6, RGD-NPs/Ce6 could significantly improve the cellular uptake capacities of DOX and Ce6 which resulted in the increased contents of ROS in cancer cells and an effective

cytotoxicity of RGD-NPs/Ce6 upon a laser radiation. Based on the active targeting mediated by NRP-1 receptor, it could effectively promote the tumor accumulations *in vivo*, and thus exhibit superior anti-tumor effect with a laser radiation in MDA-MB-231 tumor nude mice. Furthermore, the cardiotoxicity induced by free DOX was also thoroughly eradicated by this platform. In summary, the targeted chemo-photodynamic combination therapeutic platform we constructed exhibited a great potential in tumor imaging and simultaneous combined therapy against tumors.

■ ASSOICATED CONTENT

Supporting Information

synthesis route of CGRDK-PEG-DOX conjugate, cellular uptakes of NPs/Ce6 and RGD-NPs/Ce6 in MCF-7 cells, blood clearance kinetics curves of various Ce6 formulations, and H&E staining images of controlled groups.

■ AUTHOR INFORMATION

Corresponding Authors

*Email: *chulp89@163.com (Liping Chu)*

*Email: *liujinjian2002@163.com (Jinjian Liu)*

Author Contributions

[#]These authors contributed equally to this work.

Notes

The authors declare no competing financial interest.

■ ACKNOWLEDGEMENTS

This work was financially supported by the NSFC Fundings (No. 81471727, 51603231), CAMS Initiative for Innovative Medicine (2016-I2M-3-022), the Natural Science Foundation of Tianjin (16ZXXYSY00040, 16JCZDJC33000, 16JCQNJC02500), PUMC Youth Fund and the Fundamental Research Funds for the Central Universities (3332016098), and the Fundamental Research Funds for CAMS & PUMC (2016ZX310071).

■ REFERENCES

(1) Chen, W.; Zheng, R.; Baade, P. D.; Zhang, S.; Zeng, H.; Bray, F.; Jemal, A.; Yu, X. Q.; He, J. Cancer Statistics in China. 2015. *CA-Cancer J. Clin.* **2016,** *66* (2), 115-132.

(2) Chen, Q.; Xu, L.; Liang, C.; Wang, C.; Peng, R.; Liu, Z. Photothermal Therapy with Immune-adjuvant Nanoparticles Together with Checkpoint Blockade for Effective Cancer Immunotherapy. *Nat. Commun.* **2016,** *7*, 13193.

(3) Flemming, A. Autoimmunity: Nanoparticles Engineered for Antigen-specific Immunotherapy. *Nat. Rev. Immunol.* **2016,** *16* (4), 204-205.

(4) Lebel, M. E.; Chartrand, K.; Tarrab, E.; Savard, P.; Leclerc, D.; Lamarre, A. Potentiating Cancer Immunotherapy Using Papaya Mosaic Virus-Derived Nanoparticles. *Nano Lett.* **2016,** *16* (3), 1826-1832.

(5) Wang, C.; Xu, L.; Liang, C.; Xiang, J.; Peng, R.; Liu, Z. Immunological Responses Triggered by Photothermal Therapy with Carbon Nanotubes in Combination with Anti-CTLA-4 Therapy to Inhibit Cancer Metastasis. *Adv. Mater.* **2014,** *26* (48), 8154-8162.

(6) Chung, M. J.; Kim, Y. S.; Kim, J. Y.; Lee, Y. H.; Jang, J. H.; Kang, J. H.; Yoo, I. R.; Lee, Y. S. Predictors of Distant Metastasis after Radical Surgery Followed by Postoperative

Radiotherapy with or without Chemotherapy for Oropharyngeal Cancer. *Cancer Res. Treat.* **2016,** *48* (4), 1167-1176.

(7) Im, J. H.; Seong, J.; Lee, I. J.; Park, J. S.; Yoon, D. S.; Kim, K. S.; Lee, W. J.; Park, K. R. Surgery Alone Versus Surgery Followed by Chemotherapy and Radiotherapy in Resected Extrahepatic Bile Duct Cancer: Treatment Outcome Analysis of 336 Patients. *Cancer Res. Treat.* **2016,** *48* (2), 583-595.

(8) Lin, H. X.; Hua, Y. J.; Chen, Q. Y.; Luo, D. H.; Sun, R.; Qiu, F.; Mo, H. Y.; Mai, H. Q.; Guo, X.; Xian, L. J.; Hong, M. H.; Guo, L. Randomized Study of Sinusoidal Chronomodulated Versus Flat Intermittent Induction Chemotherapy with Cisplatin and 5-fluorouracil Followed by Traditional Radiotherapy for Locoregionally Advanced Nasopharyngeal Carcinoma. *Chin. J. Cancer.* **2013,** *32* (9), 502-511.

(9) Zhang, W.; Mao, J. H.; Zhu, W.; Jain, A. K.; Liu, K.; Brown, J. B.; Karpen, G. H. Centromere and Kinetochore Gene Misexpression Predicts Cancer Patient Survival and Response to Radiotherapy and Chemotherapy. *Nat. Commun.* **2016,** *7*, 12619.

(10) O'Brien, M. E.; Wigler, N.; Inbar, M.; Rosso, R.; Grischke, E.; Santoro, A.; Catane, R.; Kieback, D. G.; Tomczak, P.; Ackland, S. P.; Orlandi, F.; Mellars, L.; Alland, L.; Tendler, C.; Group, C. B. C. S. Reduced Cardiotoxicity and Comparable Efficacy in a Phase III Trial of Pegylated Liposomal Doxorubicin HCl (Caelyx/Doxil) Versus Conventional Doxorubicin for First-line Treatment of Metastatic Breast Cancer. *Ann. Oncol.* **2004,** *15* (3), 440-449.

(11) Injac, R.; Perse, M.; Cerne, M.; Potocnik, N.; Radic, N.; Govedarica, B.; Djordjevic, A.; Cerar, A.; Strukelj, B. Protective effects of fullerenol C60(OH)24 against Doxorubicin-Induced Cardiotoxicity and Hepatotoxicity in Rats with Colorectal Cancer. *Biomaterials* **2009,** *30* (6), 1184-1196.

(12) Arola, O. J.; Saraste, A.; Pulkki, K.; Kallajoki, M.; Parvinen, M.; Voipio-Pulkki, L.-M., Acute Doxorubicin Cardiotoxicity Involves Cardiomyocyte Apoptosis. *Cancer Res.* 2000, *60* (7), 1789-1792.

(13) Wang, H.; Luo, Z.; Wang, Y.; He, T.; Yang, C.; Ren, C.; Ma, L.; Gong, C.; Li, X.; Yang,

Z. Enzyme-Catalyzed Formation of Supramolecular Hydrogels as Promising Vaccine Adjuvants. *Adv. Funct. Mater.* **2016,** *26*, 1822–1829.

(14) Wang, W.; Deng, L.; Xu, S.; Zhao, X.; Lv, N.; Zhang, G.; Gu, N.; Hu, R.; Zhang, J.; Liu, J.; Dong, A. A Reconstituted "two into one" Thermosensitive Hydrogel System Assembled by Drug-loaded Amphiphilic Copolymer Nanoparticles for the Local Delivery of Paclitaxel. *J. Mater. Chem. B* **2013,** *1* (4), 552-563.

(15) Cheng, T.; Liu, J.; Ren, J.; Huang, F.; Ou, H.; Ding, Y.; Zhang, Y.; Ma, R.; An, Y.; Liu, J.; Shi, L. Green Tea Catechin-Based Complex Micelles Combined with Doxorubicin to Overcome Cardiotoxicity and Multidrug Resistance. *Theranostics* **2016,** *6* (9), 1277-1292.

(16) Huang, F.; Wang, J.; Qu, A.; Shen, L.; Liu, J.; Liu, J.; Zhang, Z.; An, Y.; Shi, L. Maintenance of Amyloid Beta Peptide Homeostasis by Artificial Chaperones Based on Mixed-Shell Polymeric Micelles. *Angew. Chem. Int. Ed.* **2014,** *53* (34), 8985-8990.

(17) Kuang, Y.; Xu, B. Disruption of the Dynamics of Microtubules and Selective Inhibition of Glioblastoma Cells by Nanofibers of Small Hydrophobic Molecules. *Angew. Chem. Int. Ed.* **2013,** *52* (27), 6944-6948.

(18) Wang, H.; Feng, Z.; Xu, B. D-amino Acid-Containing Supramolecular nanofibers for Potential Cancer Therapeutics. *Adv. Drug Deliv. Rev.* **2016,** doi: 10.1016/j.addr.2016.04.008.

(19) Miao, Q.; Lyu, Y.; Ding, D.; Pu, K. Semiconducting Oligomer Nanoparticles as an Activatable Photoacoustic Probe with Amplified Brightness for *in vivo* Imaging of pH. *Adv. Mater.* **2016,** *28* (19), 3662-3668.

(20) Song, Z.; Mao, D.; Sung, S. H.; Kwok, R. T.; Lam, J. W.; Kong, D.; Ding, D.; Tang, B. Z. Activatable Fluorescent Nanoprobe with Aggregation-Induced Emission Characteristics for Selective *in vivo* Imaging of Elevated Peroxynitrite Generation. *Adv. Mater.* **2016,** *28* (33), 7249-7256.

(21) Cai, T.; Lei, Q.; Yang, B.; Jia, H. Z.; Cheng, H.; Liu, L. H.; Zeng, X.; Feng, J.; Zhuo, R. X.; Zhang, X. Z. Utilization of H-Bond Interaction of Nucleobase Uralic with Antitumor

Methotrexate to Design Drug Carrier with Ultrahigh Loading Efficiency and pH Responsive Drug Release. *Regener. Biomater.* **2014,** 1, 27-35.

(22) Drozd, E.; Krzyszton-Russjan, J.; Gruber, B. Doxorubicin Treatment of Cancer Cells Impairs Reverse Transcription and Affects the Interpretation of RT-qPCR Results. *Cancer Genomics Proteomics* **2016,** *13* (2), 161-70.

(23) Jeon, M. J.; Gordon, A. C.; Larson, A. C.; Chung, J. W.; Kim, Y. I.; Kim, D. H. Transcatheter Intra-arterial Infusion of Doxorubicin Loaded Porous Magnetic Nano-Clusters with Iodinated Oil for the Treatment of Liver Cancer. *Biomaterials* **2016,** *88*, 25-33.

(24) Tsai, L. C.; Hsieh, H. Y.; Lu, K. Y.; Wang, S. Y.; Mi, F. L. EGCG/gelatin-Doxorubicin Gold Nanoparticles Enhance Therapeutic Efficacy of Doxorubicin for Prostate Cancer Treatment. *Nanomedicine* **2016,** *11* (1), 9-30.

(25) Lu, J.; Zhao, W.; Liu, H.; Marquez, R.; Huang, Y.; Zhang, Y.; Li, J.; Xie, W.; Venkataramanan, R.; Xu, L.; Li, S. An Improved D-alpha-tocopherol-Based Nanocarrier for Targeted Delivery of Doxorubicin with Reversal of Multidrug Resistance. *J. controlled release* **2014**, *196*, 272-286.

(26) Hu, C. M.; Aryal, S.; Zhang, L. Nanoparticle-Assisted Combination Therapies for Effective Cancer Treatment. *Ther. Delivery* **2010,** *1* (2), 323-34.

(27) Huan Meng, H. Z., Min Xue, Tian Xia, Sijie Lin, Xiang Wang, Yang Zhao, Zhaoxia Ji, Jeffrey I. Zink, and Andre E. Nel Codelivery of an Optimal Drug/siRNA Combination Using Mesoporous Silica Nanoparticles to Overcome Drug Resistance in Breast Cancer *in vitro* and *in vivo*. *ACS Nano* **2013,** *7* (2), 994-1005.

(28) Li, K.; Liu, H.; Gao, W.; Chen, M.; Zeng, Y.; Liu, J.; Xu, L.; Wu, D. Mulberry-Like Dual-Drug Complicated Nanocarriers Assembled with Apogossypolone Amphiphilic Starch Micelles and Doxorubicin Hyaluronic Acid Nanoparticles for Tumor Combination and Targeted Therapy. *Biomaterials* **2015,** *39*, 131-144.

(29) Huang, P.; Zhang, Y.; Wang, W.; Zhou, J.; Sun, Y.; Liu, J.; Kong, D.; Liu, J.; Dong, A.

Co-Delivery of Doxorubicin and (131)I by Thermosensitive Micellar-hydrogel For Enhanced in Situ Synergetic Chemoradiotherapy. *J. controlled release* **2015**, *220* (Pt A), 456-464.

(30) He, C.; Liu, D.; Lin, W. Self-Assembled Core-Shell Nanoparticles for Combined Chemotherapy and Photodynamic Therapy of Resistant Head and Neck Cancers. *ACS Nano* **2015,** *9* (1), 991-1003.

(31) Hou, W.; Zhao, X.; Qian, X.; Pan, F.; Zhang, C.; Yang, Y.; de la Fuente, J. M.; Cui, D. pH-Sensitive Self-assembling Nanoparticles for Tumor Near-infrared Fluorescence Imaging and Chemo-photodynamic Combination Therapy. *Nanoscale* **2016,** *8* (1), 104-116.

(32) Jiang, D.; Gao, X.; Kang, T.; Feng, X.; Yao, J.; Yang, M.; Jing, Y.; Zhu, Q.; Feng, J.; Chen, J. Actively Targeting D-alpha-tocopheryl Polyethylene Glycol 1000 Succinate-poly(lactic acid) Nanoparticles as Vesicles for Chemo-photodynamic Combination Therapy of Doxorubicin-resistant Breast Cancer. *Nanoscale* **2016,** *8* (5), 3100-3118.

(33) Suzuki, F.; Misawa, M.; Sugimura, H.; Yamawaki, S.; Aoshima, M. Efficacy of Photodynamic Therapy Combined with a Guide Sheath Method Concomitant with Chemotherapy in a Small-cell Lung Cancer Patient with Central Endobronchial Stenosis. *Photodiagn. Photodyn. Ther.* **2016,** *16*, 169-171.

(34) Thapa, P.; Li, M.; Bio, M.; Rajaputra, P.; Nkepang, G.; Sun, Y.; Woo, S.; You, Y. Far-Red Light-Activatable Prodrug of Paclitaxel for the Combined Effects of Photodynamic Therapy and Site-Specific Paclitaxel Chemotherapy. *J. Med. Chem.* **2016,** *59* (7), 3204-3214.

(35) Wang, Z.; Ma, R.; Yan, L.; Chen, X.; Zhu, G. Combined Chemotherapy and Photodynamic Therapy Using a Nanohybrid Based on Layered Double Hydroxides to Conquer Cisplatin resistance. *Chem. Commun.* **2015,** *51* (58), 11587-11590.

(36) Yang, Y.; Yu, M.; Song, H.; Wang, Y.; Yu, C. Preparation of Fluorescent Mesoporous Hollow Silica-fullerene Nanoparticles Via Selective Etching for Combined Chemotherapy and Photodynamic Therapy. *Nanoscale* **2015,** *7* (28), 11894-11898.

(37) Desgrosellier, J. S.; Cheresh, D. A. Integrins in Cancer: Biological Implications and

Therapeutic Opportunities. *Nat. Rev. Cancer* **2010,** *10* (1), 9-22.

(38) Vanneman, M.; Dranoff, G. Combining Immunotherapy and Targeted Therapies in Cancer Treatment. *Nat. Rev. Cancer* **2012,** *12* (4), 237-251.

(39) Sugahara, K. N.; Teesalu, T.; Karmali, P. P.; Kotamraju, V. R.; Agemy, L.; Greenwald, D. R.; Ruoslahti, E. Coadministration of a Tumor-Penetrating Peptide Enhances the Efficacy of Cancer Drugs. *Science* **2010,** *328* (5981), 1031-1035.

(40) Kumar, A.; Huo, S.; Zhang, X.; Liu, J.; Tan, A.; Li, S.; Jin, S.; Xue, X.; Zhao, Y.; Ji, T.; Han, L.; Liu, H.; Zhang, X.; Zhang, J.; Zou, G.; Wang, T.; Tang, S.; Liang, X. J. Neuropilin-1-Targeted Gold Nanoparticles Enhance Therapeutic Efficacy of Platinum(IV) Drug for Prostate Cancer Treatment. *ACS Nano* **2014,** *8* (5), 4205-4220.

(41) Kumar, A.; Ma, H.; Zhang, X.; Huang, K.; Jin, S.; Liu, J.; Wei, T.; Cao, W.; Zou, G.; Liang, X. J. Gold Nanoparticles Functionalized with Therapeutic and Targeted Peptides for Cancer Treatment. *Biomaterials* **2012,** *33* (4), 1180-1189.

(42) Zhang, Y.; Yang, C.; Wang, W.; Liu, J.; Liu, Q.; Huang, F.; Chu, L.; Gao, H.; Li, C.; Kong, D.; Liu, Q.; Liu, J. Co-Delivery of Doxorubicin and Curcumin by pH-Sensitive Prodrug Nanoparticle for Combination Therapy of Cancer. *Sci. Rep.* **2016,** *6*, 21225.

(43) Delplace, V.; Couvreur, P.; Nicolas, J. Recent Trends in The Design of Anticancer Polymer Prodrug Nanocarriers. *Polym. Chem.* **2014,** *5* (5), 1529-1544.

(44) Huang, P.; Liu, J.; Wang, W.; Li, C.; Zhou, J.; Wang, X.; Deng, L.; Kong, D.; Liu, J.; Dong, A. Zwitterionic Nanoparticles Constructed with Well-defined Reduction-Responsive Shell and pH-Sensitive Core for "Spatiotemporally Pinpointed" Drug Delivery. *ACS Appl. Mater. Interfaces* **2014,** *6* (16), 14631-14643.

(45) Cabral, H.; Matsumoto, Y.; Mizuno, K.; Chen, Q.; Murakami, M.; Kimura, M.; Terada, Y.; Kano, M. R.; Miyazono, K.; Uesaka, M.; Nishiyama, N.; Kataoka, K. Accumulation of Sub-100 nm Polymeric Micelles in Poorly Permeable Tumours Depends on Size. *Nat. Nanotechnol.* **2011,** *6* (12), 815-823.

(46) Keizer, H. G.; Pinedo, H. M.; Schuurhuis, G. J.; Joenje, H. Doxorubicin (adriamycin): a Critical Review of Free Radical-Dependent Mechanisms of Cytotoxicity. *Pharmacol. Ther.* **1990,** *47* (2), 219-231.

(47) Yu, Y.; Chen, C. K.; Law, W. C.; Weinheimer, E.; Sengupta, S.; Prasad, P. N.; Cheng, C. Polylactide-graft-Doxorubicin Nanoparticles with Precisely Controlled Drug Loading for pH-triggered Drug Delivery. *Biomacromolecules* **2014,** *15* (2), 524-532.

(48) Wang, T.; Zhang, L.; Su, Z.; Wang, C.; Liao, Y.; Fu, Q. Multifunctional Hollow Mesoporous Silica Nanocages for Cancer Cell Detection and the Combined Chemotherapy and Photodynamic Therapy. *ACS Appl. Mater. Interfaces* **2011,** *3* (7), 2479-2486.

(49) Zhou, Z.; Song, J.; Nie, L.; Chen, X. Reactive Oxygen Species Generating Systems Meeting Challenges of Photodynamic Cancer Therapy. *Chem. Soc. Rev.* **2016,** *45* (23), 6597-6626.

(50) Wei, T.; Liu, J.; Ma, H.; Cheng, Q.; Huang, Y.; Zhao, J.; Huo, S.; Xue, X.; Liang, Z.; Liang, X. J. Functionalized Nanoscale Micelles Improve Drug Delivery for Cancer Therapy *in vitro* and *in vivo*. *Nano Lett.* **2013,** *13* (6), 2528-2534.

(51) Chen, Q.; Feng, L.; Liu, J.; Zhu, W.; Dong, Z.; Wu, Y.; Liu, Z. Intelligent Albumin-MnO2 Nanoparticles as pH-/H2O2-Responsive Dissociable Nanocarriers to Modulate Tumor Hypoxia for Effective Combination Therapy. *Adv. Mater.* **2016,** *28* (33), 7129-7136.

(52) Liu, J; Deng, H; Liu, Q; Chu, L; Zhang, Y; Yang, C; Zhao, X; Huang, P; Deng, L; Dong, A; Liu, J. Integrin-Targeted pH-Responsive Micelles for Enhanced Efficiency of Anticancer Treatment *in vitro* and *in vivo*. *Nanoscale* **2015,** *7* (10), 4451-4460.

Table of Contents (TOC)

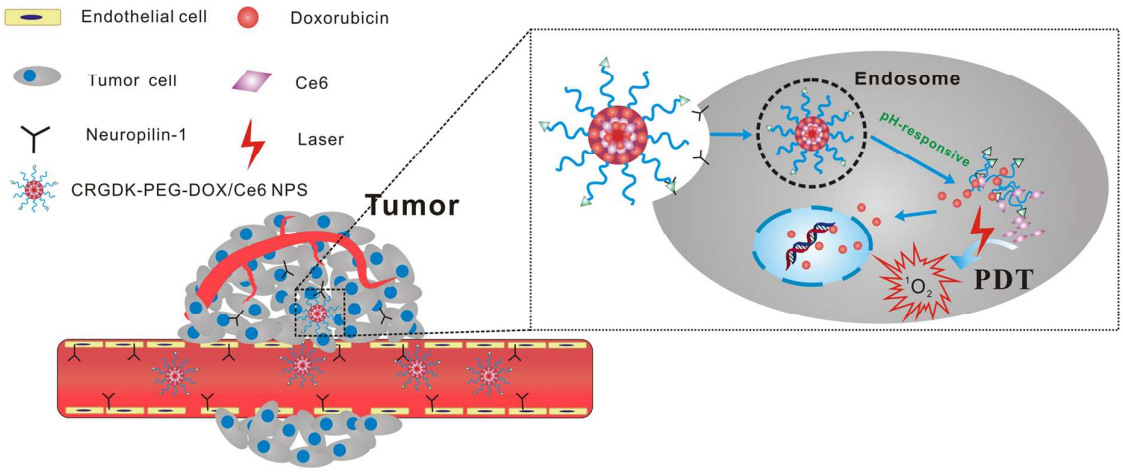
Endothelial cell
Doxorubicin
Tumor cell
Ce6
Neuropilin-1
Laser
CRGDK-PEG-DOX/Ce6 NPS
Tumor
Endosome
pH-responsive
$^1O_2$
PDT